10.1109/JSEN.2015.2443012

Effects of Wind-induced Near-surface Bubble Plumes on the Performance of Underwater Wireless Acoustic Sensor Networks

Amit Kumar Mandal, Sudip Misra, *Senior Member, IEEE,* Tamoghna Ojha, *Student Member, IEEE,* Mihir Kumar Dash, Mohammad S. Obaidat, *Fellow, IEEE*

***Abstract*—This paper analyzes the effects of near-surface oceanic bubble plumes on the overall performance of Underwater Wireless Acoustic Sensor Networks (UWASNs). The existence of bubble plumes in surface and sub-surface ocean water columns is inevitable in most windy oceanic environments. There exists studies reporting the anomalous behavior of acoustic signal propagating through oceanic bubble plumes due to absorption and scattering. However, most of the existing network protocols designed for use in UWASNs are ignorant of these effects. In this paper, we first mathematically model the absorption effects of these bubble plumes on the acoustic communication media. Consequently, the overall performance of UWASNs is studied with respect to different parameters. Simulation based results show that in the presence of bubble plumes, packet delivery ratio decreases by 34% while average energy consumption per node increases by 7%. Also, SINR decreases by approximately 53% and BER increases by 57% in the presence of bubble plumes in UWASNs.**

***Index Terms*—Underwater wireless acoustic sensor networks, bubble plumes, path loss, acoustic communication**

I. Introduction

A UWASN consists of variable number of sensor nodes, which are capable of sensing, processing, and communicating, and are deployed over a given area of interest to perform application-specific tasks [1], [2]. UWASNs are envisioned to enable applications such as oceanographic data collection, pollution monitoring, offshore exploration, disaster prevention, and assisted navigation [1], [2]. Large volume of research literature (e.g., [1]–[7]) exists on UWASNs and related fields.

A. Motivation

Unlike terrestrial wireless sensor networks, UWASNs suffer from multiple challenges [8], [9]. In addition to having common factors, such as path loss, noise, and multi-path fading, inter-node acoustic communication is greatly affected due to the presence of other physical phenomena, like wind-induced near-surface bubble plumes. Under the deployment of UWASNs in windy environments, inclusion of the effects of bubble plumes is hard to ignore. However, to the best of our knowledge, the existing literature ignored the effects of bubble plumes on the overall network performance, despite the fact that the existence of near-surface bubble plumes is inevitable in most windy oceanic environments. This work is an attempt towards addressing this important research lacuna.

An ocean column is typically segmented into three layers – *mixed*, *thermocline*, and *deep isothermal*. Among all these layers, the mixed layer is normally the most turbulent [10]. The upper surface of this layer is directly subjected to tangential stress due to surface winds. In other words, the transfer of momentum takes place from wind to the water surface, which often results in splashing/breaking of waves. This phenomenon creates concentrated layers of micro-bubbles underlying the ocean surface, typically upto a depth of 10 m [11]. The layers of bubble plumes have been observed to vary not only in depth, but also in range and time [12]. Their evolution in density, radius, and spatial distribution has impact on the quality of acoustic communication [13].

B. Contributions

The performance of UWASNs is very sensitive to the presence of near-surface bubble plumes. Again, the wind has an important role on the nature and intensity of plumes at subsurface region. Therefore, it is important to study the effect of wind velocity on the overall performance of UWASNs. In brief, the *contributions* of this work are catalogued bellow as:

- We have modelled the impact of subsurface bubbles on the performance of UWASNs.
- We have analyzed the effects of wind speed on formation of subsurface bubble plumes which in turn affects the performance of UWASNs.
- We have evaluated the performance of the UWASNs in terms of various metrics – packet delivery ratio, SINR, BER, and average energy consumption per node.

The rest of the paper is organized as follows. In Section II, we briefly review the related literature. We present the communication architecture of our proposed framework in Section III. The detailed characterization of bubble plumes and various factors affecting them are discussed in Section IV. Next, in Section V, we analytically model the communication between underwater nodes affected by bubble plumes. The simulation results of our proposed model is presented in

A. K. Mandal and M. K. Dash are with the Center for Oceans, Rivers, Atmosphere and Land Sciences, Indian Institute of Technology Kharagpur, WB, 721302, India. E-mail: amiit.mandal@gmail.com, mihir@coral.iitkgp.ernet.in

S. Misra and T. Ojha are with the School of Information Technology, Indian Institute of Technology Kharagpur, WB, 721302, India. E-mail: {smisra, tojha}@sit.iitkgp.ernet.in

M. S. Obaidat is with the Department of Computer Science and Software Engineering, Monmouth University, West Long Branch, NJ 07764, USA. Email: obaidat@monmouth.edu

Section VI. Finally, the paper concludes in Section VII citing directions for future works.

II. Related Work

Ismail et al. [14] analyzed the performance of UWASNs in terms of propagation loss by considering the acoustic signal to be propagated through underwater ocean channel. The authors considered only the inherent characteristics of the underwater channel from the communication point of view. They did not consider the effect of bubble plumes on the communication performance. Stefanov and Stojanovic [15] analyzed the performance of underwater acoustic ad-hoc networks in the presence of interference. They assumed uniform distribution of nodes in the entire channel. In this work, the authors modelled the signal path loss in inter-node communication to be frequency dependent, and considered Rician distribution of acoustic fading. A recent work by Mandal et al. [16] studied the acoustic signal perturbation characteristics due to the presence of near-surface bubble plumes in underwater environments. However, they did not consider the effect of plumes on the overall performance of underwater sensor networks.

Fox et al. [17] proposed a methodology for predicting the underwater acoustic communication performance. They showed how performance varies with respect to the variation in relative locations of source and receiver nodes in the perspective of acoustic speed profile in the channel. The authors have considered parameters such as variable sound speed profiles as a function of environment variables between the source and the receiver nodes. These parameters help in assessing the overall communication performance of UWASNs. Llor and Malumbes [18] studied how physical layer modelling affects the performance of higher layer protocols. Zhang et al. [19] considered a linear multi-hop communication architecture to model acoustic propagation. They took into account frequency-dependent signal attenuation, inter-hop interference, and propagation delay.

Synthesis of the review of existing works reveals the absence of any study on the performance analysis of UWASNs in the presence of near-surface bubble plumes. However, under the deployment of sensor networks in a windy state ocean, the effect of near-surface bubble plumes on the overall network performance of UWASNs is unavoidable.

III. Communication Architecture

We have considered a 3-D architecture, where the sensor nodes (N) are randomly distributed under water, as shown in Fig. 1. We have considered three types of nodes – the *sink*, the *relay* and the *source* nodes. The sink node is deployed at the ocean surface. We have considered the seabed nodes as the information source. The nodes placed in between the source and surface sink nodes act as the relay nodes. These relay nodes help in routing information from the source node to the surface sink. The sensed information by these nodes are communicated to the surface sink following a multi-hop path.

All the deployed nodes are assumed to be homogeneous in nature with respect to their transmission capability. Let the transmission range of any node is r. Connectivity between any two nodes is established when they are in the transmission range of each other. Mathematically, $d_{ij} \leq r$, where d_{ij} is the distance between node N_i and N_j. The network model is represented as a graph $G(N, E_{ij})$, where $N = N_1, N_2, ..., N_n$ is the set of all underwater nodes deployed in the 3-D ocean space, and E_{ij} is the link established between two nodes N_i and N_j. Mathematically, $(N_i, N_j) \in E_{ij} \quad \forall d_{ij} \leq r$.

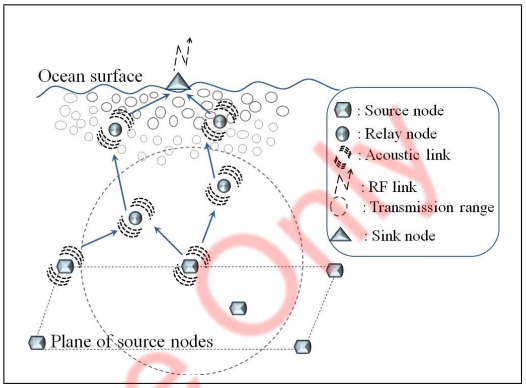

Fig. 1: Communication architecture of our proposed problem

IV. Characterization of Near-surface Wind-induced Bubble Plumes

In this section, we categorize the near-surface bubble plumes according to their physical characteristics.

A. Categorization of Bubble Plumes

The physical unit formed by the combination of many discrete bubbles is termed as *bubble plume* or *bubble clouds* [20]. Based on Thorp's measurements and observations [20], Monahan [21] classified bubble plumes into three categories: α, β, and γ. These plumes bear their names on the basis of their individual lifetime during active bubble generation process induced by wind action on the ocean surface.

These $\beta-$plumes, typically, persist only upto 4 seconds. In course of time, the $\beta-$plumes evolve into $\gamma-$plumes, and gradually become detached from the originating whitecap. Among the three plume categories, $\gamma-$plumes have the lowest void fraction ranging from 10^{-6} to 10^{-7} with a time span 10-100 times greater than $\beta-$plumes. Due to their high longevity and size, the $\gamma-$plumes are affected by the local circulation process, and finally decay to a weak-stratified background layer. Although, the $\alpha-$plumes have high void fraction, they possess very short lifetime with respect to $\beta-$ and $\gamma-$plumes. Therefore, we have *omitted* the analysis of the their effect on the performance of distributed UWASNs.

B. Physical Characterization of Bubble Plumes

This section discusses the spatial distribution of bubble plumes and the quantification of their population. Monahan [21] extensively studied the characteristics of oceanic bubbles, and their importance in the gas exchange between air-sea interface. As proposed by Hall [22], the *Bubble Population*

Spectral Density (*BPSD*), ζ, for any level of bubble plume is mathematically expressed in the functional form as:

$$\zeta(r, z, w_{10}) = N_0 \Psi(r, z) Z(z, w_{10}) W(w_{10}) \tag{1}$$

In Equation (1), r is the bubble radius, z is the depth from ocean surface, w_{10} is the wind speed 10 m[1] above the sea surface, W is a wind-dependent factor, and N_0 is a constant having value corresponding to a particular value of ζ, which is obtained for particular values of radius (r), depth (z), and wind velocity (w_{10}). The term $\Psi(r, z)$ denotes the spectral shape function, $Z(z)$ is the depth dependent function signifying the e-folding depth [23] for each level of bubble plumes. The e-folding depth is normalized with respect to the reference depth $z = 0$. Thus, the general form of Equation (1) is written as:

$$\zeta(r, z, w_{10}) = N_0 \Psi(r) Z(z) W(w_{10}) \tag{2}$$

C. Wind Dependent Factor

As observed by Monahan [21], the rate of generation of bubble plumes is equal to the rate of formation of whitecaps. The study of the relation between the fraction of whitecaps on the sea surface and the wind velocity was undertaken by Monahan and Muircheartaigh [24]. Later, Andreas and Monahan [25] showed that the fraction of whitecaps present on the sea surface can be approximated to be proportional to the third power of wind speed. Hall [22] undertook an integrated study on several research works done on the dependence of BPSD on wind velocity (w_{10}).

In the context of bubble plume generation, the wind dependent factor is mathematically expressed as in Ref. [12] [22]:

$$W(w_{10}) = (\frac{w_{10}}{13})^3 \tag{3}$$

Here, the assumption is that wind is the main factor to induce the formation of all bubbles, the function $W(w_{10})$ is regarded the same for all stages of plume development, including the last stage, i.e., the background layer at any instant of time.

Wind velocity is an important factor in deciding the penetration depth of a particular type of plume. It is usually seen that penetration depth of $\beta-$Plume is lower that of the penetration depth of $\gamma-$Plume for a particular wind velocity. Variation of penetration depth for both types of aforementioned plumes are shown in Fig. 2.

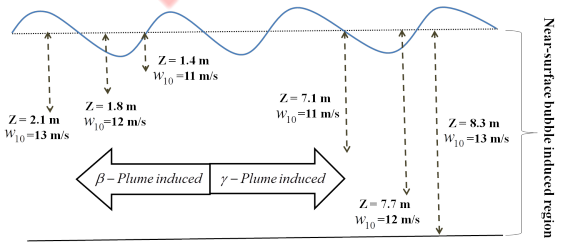

Fig. 2: Variation of penetration depths of plumes with the variation in wind speed

[1]It has the most significant effect on near-surface bubble plume generation.

D. Nature of Spectral Shape Function

Based on the analysis of several experimental data using multiple measuring techniques, Hall [22] postulated that the spectral shape function follows power law with an exponent close to -4. It has been observed that this power law is valid for bubbles having radii in the range 20-30 μm upto 50-80 μm. Again, on the basis of the report presented by Hall [22], it can be stated that the power law for spectral shape function holds good for small and intermediate shaped bubbles. Therefore, power law of spectral shape function is invariant for small and intermediate sized bubbles, except for the changes in population size.

The generalized form of the spectral shape function for $\beta-$plumes, $\gamma-$plumes, and the background layer is expressed as [22]:

$$\Psi(r) = \begin{cases} 0, & \text{for } r_{ref} < r_{min} \\ (\frac{r_{ref}}{r_1})^3, & \text{for } r_{min} \leq r_{ref} < r_1 \\ 1.0, & \text{for } r_1 \leq r_{ref} \geq r_2 \\ (\frac{r_2}{r_{ref}})^4, & \text{for } r_2 < r_{ref} \leq r_3 \end{cases} \tag{4}$$

In Equation (4), r_{min} = 10 μm, r_1 = 15 μm, r_2 = 20 μm, r_3 = 54.4 + (1.984)z μm, and z is in meter. In the subsequent sections, BPSD for different types of bubble plumes is discussed.

1) Form of BPSD for $\beta-$Plume: The functional form of BPSD for $\beta-$plumes is expressed as [12]:

$$\zeta_\beta(r, z, w_{10}) = N_{0\beta} \Psi_\beta(r) Z_\beta(z) W(w_{10}) \tag{5}$$

In Equation (5), the value of the constant, $N_{0\beta}$, is taken to be 2.0$\times 10^7$ $m^{-3}\mu m^{-1}$ [23]. The functional form for spectral shape function, $\Psi_\beta(r)$, for $\beta-$plume can be expressed as:

$$\Psi_\beta(r_{ref}) = \begin{cases} 0, & \text{for } r_{ref} < r_{min} \\ (\frac{r_{ref}}{r_1})^3, & \text{for } r_{min} \leq r_{ref} < r_1 \\ 1.0, & \text{for } r_1 \leq r_{ref} \geq r_2 \\ (\frac{r_2}{r_{ref}})^4, & \text{for } r_2 < r_{ref} \geq r_3 \\ (\frac{r_2}{r_3})^4 (\frac{r_3}{r_{ref}})^{2.6}, & \text{for } r_{ref} > r_3 \end{cases} \tag{6}$$

Following the work by Monahan and Lu [26], which considers uniform distribution of $\beta-$plume as a function of e-folding depth, the general form of depth dependent function is mathematically expressed as:

$$Z_\beta(z_{ref}) = \begin{cases} 1.0, & \text{for } z_{ref} \leq z_{\beta max} \\ 0, & \text{for } z_{ref} > z_{\beta max} \end{cases} \tag{7}$$

In Equation (7), the parameter, $Z_{\beta max}$, refers to the maximum penetration depth of a $\beta-$plume, and it is related to orbital motion of breaking wave. Therefore, it controls the vertical axis of $\beta-$plume. Normally, the penetration depth of $\beta-$plume extends to one half of the significant wave height [23]. The expression of maximum penetration depth for $\beta-$plume, $Z_{\beta max}$, is presented as in Ref. [12]:

$$Z_{\beta max} = (1.23 \times 10^2) w_{10}^2 \tag{8}$$

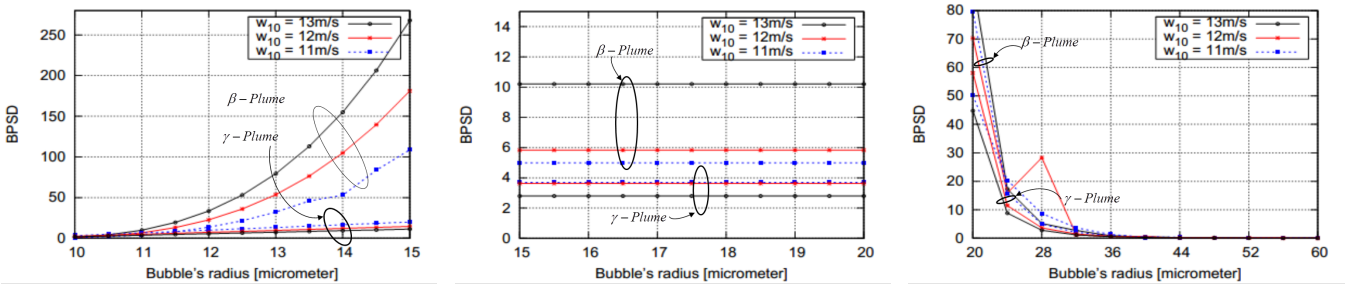

(a) BPSD for small and intermediate bubbles (b) BPSD for near-large bubbles (c) BPSD for large bubbles

Fig. 3: Distribution of BPSD for $\beta-$ and $\gamma-$plumes

2) BPSD for $\gamma-$plume: Mathematically, bubble density spectrum for $\gamma-$plume can be expressed in a manner similar to that in Equation (5) for $\beta-$plume. Therefore, considering various parameters associated with the $\gamma-$plume, the density spectrum is expressed as:

$$\zeta_\gamma(r, z, w_{10}) = N_{0\gamma}\Psi_\gamma(r)Z_\gamma(z)W(w_{10}) \tag{9}$$

As $\gamma-$plumes are the transformed products of $\beta-$plumes, the spectral shape function of $\gamma-$plumes, $\Psi_\gamma(r)$, for small and intermediate shaped bubbles remains unchanged. However, their concentration gets weaker. During the transformation phase from $\beta-$plume to $\gamma-$plume, a significant change is observed in bubble population size.

The spectral shape function for $\gamma-$plume is expressed as in [12]:

$$\Psi_\gamma(r_{ref}) = \begin{cases} 0, & \text{for } r_{ref} < r_{min} \\ (\frac{r_{ref}}{r_1}), & \text{for } r_{min} \le r_{ref} < r_1 \\ 1.0, & \text{for } r_1 \le r_{ref} \ge r_2 \\ (\frac{r_2}{r_{ref}})^4, & \text{for } r_2 < r_{ref} \le r_3 \\ (\frac{r_2}{r_3})^4(\frac{r_3}{r_{ref}})^{p(z)}, & \text{for } r_{ref} > r_3 \end{cases} \tag{10}$$

In Equation (10), $p(z)$ is the spectral slope, which has a steeper value for the bubbles having radius larger than 60 μm, and it is expressed as:

$$p(z) = 4.37 + (\frac{z}{2.55})^2 \tag{11}$$

Figs. 3 (a), (b), (c) depict the distribution of BPSD for both the plumes. From the figures, we observe that the distribution curves get shifted upward for $\beta-$plume with respect to the $\gamma-$plume.

E. Nature of Penetration of $\beta-$ and $\gamma-$plumes

Wind velocity is an important factor in deciding the penetration depth of a particular type of plume. It is usually seen that the penetration depth of $\beta-$plume is lower than that of the $\gamma-$plume for a particular wind velocity.

Wireless acoustic signal propagates partly through the $\gamma-$plume induced region and partly through the $\beta-$ and $\gamma-$plume induced regions, together. Fig. 4 shows the bubble induced regions under different wind speeds.

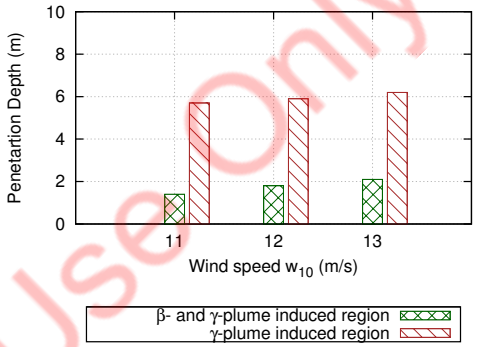

Fig. 4: Bubble induced regions under different wind speed

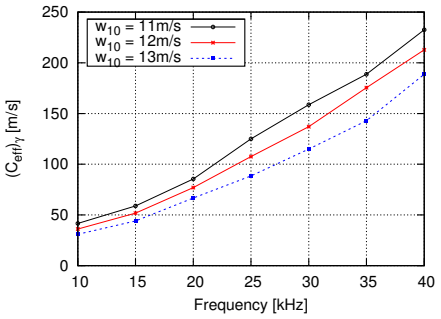

(a) Effective speed, $(C_{eff})_\gamma$, of acoustic signal through Gamma plume

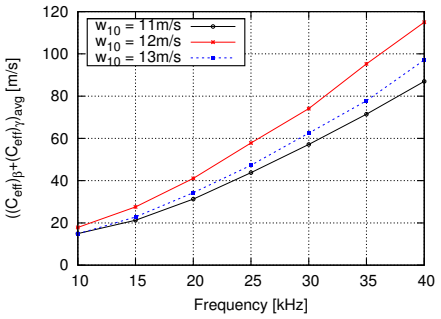

(b) Effective speed of acoustic signal through Beta as well as Gamma-plume

Fig. 5: Acoustic signal propagation through $\beta-$ and $\gamma-$plume induced region

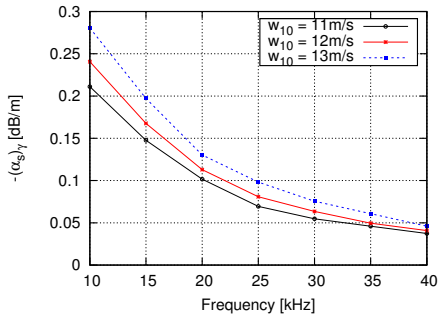

(a) Attenuation, $(\alpha_s)_\gamma$ of acoustic signal through Gamma plume

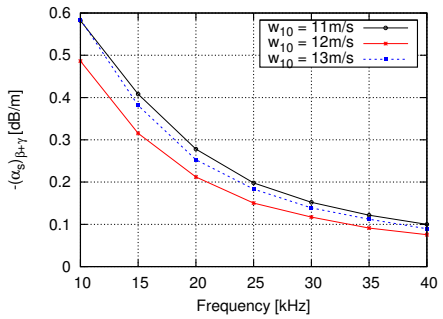

(b) Attenuation of acoustic signal due to combined effect of Beta and Gamma plume

Fig. 6: Attenuation of acoustics signal through $\beta-$ and $\gamma-$plume

V. Proposed Analytical Modeling of the Acoustic Signal in the Presence of Bubble Plumes

During propagation through oscillating bubble clouds, acoustic signal gets attenuated. To calculate the attenuation and perturbation caused by bubble plumes, we followed the approach used by Norton and Novarini [12] and Hall [22]. The assumptions made in these approaches are as follows:

- The compressional speed of acoustic signal is assumed to be approximately constant throughout the medium.
- There is no interaction between any group of bubbles.
- Due to the oscillation mechanism, the medium becomes dispersive.
- Multiple scattering among the bubbles is negligible.

The effective sound speed, C_{eff}, through plume is expressed as [12]:

$$\frac{1}{C_{eff}^2} = \frac{1}{C_0^2} + \frac{1}{\pi f^2}\int_{r_{min}}^{r_{max}} \left[\frac{r\zeta(r)}{((\frac{f_r}{f})^2 - 1 + i\delta)}\right] dr \qquad (12)$$

where, $\delta = \delta_r = \frac{2\pi f r}{C_0}$, is effective damping through plume, C_0 is speed of free channel propagation of acoustic signal, $f_r = (1+\frac{z}{10})^{0.5}(\frac{3.25\times10^6}{r})$ is resonance frequency of bubbles.

Further calculation on the Equation (12) yields to Equation (13) as:

$$\frac{1}{C_{eff}^2} = \frac{1}{C_0^2} + \frac{1}{\pi f^2}\int_{r_{min}}^{r_{max}} \frac{r\zeta(r)[((\frac{f_r}{f})^2 - 1) - i\delta_r]}{[((\frac{f_r}{f})^2 - 1)^2 + \delta_r^2]} dr \qquad (13)$$

Simplifying Equation (13), we can write:

$$\frac{1}{C_{eff}^2} = \frac{1}{C_0^2} + \frac{1}{\pi f^2}\int_{r_{min}}^{r_{max}} \frac{r\zeta(r)[((\frac{f_r}{f})^2 - 1)]}{[((\frac{f_r}{f})^2 - 1)^2 + \delta_r^2]} dr \qquad (14)$$

$$\frac{1}{C_{eff}^2} = \frac{1}{C_0^2} + \frac{1}{\pi f^2}\int_{r_{min}}^{r_{max}} \frac{r\zeta(r)(-\delta_r)}{[((\frac{f_r}{f})^2 - 1)^2 + \delta_r^2]} dr \qquad (15)$$

Equations (14) and (15), respectively, represent the real and imaginary parts. Next, we analyze the sound speed modified during propagation through $\beta-$ and $\gamma-$plumes.

A. Sound Speed Perturbation by $\beta-$ and $\gamma-$plume

Sound perturbation due to bubble plume depends on the wind speed and the type of plume. In this section, we have computed the effective sound speed caused due to only the $\beta-$ and $\gamma-$plumes.

1) Perturbation by $\beta-$plume: On the basis of their sizes, $\beta-$plumes are classified in three subtypes: *small-and-intermediate*, *near-large*, and *large*. Contribution to the effective sound speed, C_{eff}, through $\beta-$plume comes from these three subtypes. The parameter, C_{eff}, for $\beta-$plume is expressed as:

$$(\frac{1}{C_{eff}})_\beta = \sqrt{\frac{1}{C_0^2} - I_\beta} \qquad (16)$$

In Equation (16), the quantity I_β is known as the integration term, which is expressed as:

$$I_\beta = \frac{1}{\pi f^2}\int_{r_{min}}^{r_{max}} \frac{r\varsigma_\beta(\delta_r)}{[((\frac{f_r^\beta}{f})^2 - 1)^2 + \delta_r^2]} dr \qquad (17)$$

In Equation (17), f_r^β is known as the resonance frequency of $\beta-$plume. It is a function of the bubble radius and the depth of influence of the plume.

Substituting the values of BPDS, ς_β, of $\beta-$plume, for different bubble sub-categories, we calculate the integral, I_β, for these plume subtypes. Depending on the bubble subtypes, the limits of integration are varied. For small-and-intermediate plumes, $r_{min} = r_{min}$, and $r_{max} = r_1$, for near-large, $r_{min} = r_1$ and $r_{max} = r_2$, for large, $r_{min} = r_2$ and $r_{max} = r_3$. As an example, we have evaluated the integral, I_β, for small-and-intermediate bubbles, and have denoted it as I_s.

2) Perturbation by $\gamma-$Plume: As in the case of $\beta-$plume, the $\gamma-$plume is further classified into three categories. Contribution to the effective sound speed under variable wind speed for each of these categories has been taken into consideration.

The effective sound speed, C_{eff}, through $\gamma-$plume is expressed as:

$$(\frac{1}{C_{eff}})_\gamma = \sqrt{\frac{1}{C_0^2} - I_\gamma} \qquad (18)$$

For different values of BPDS, ς_γ, of $\gamma-$plume, we integrate, I_γ for different bubble subtypes. Depending on these

subtypes, the integration limits are varied. For instance, we have evaluated the integral, I_s, for the small-and-intermediate bubbles under the wind speed, w_{10}.

B. Acoustic Signal Attenuation by Near-surface Bubble Plumes

In Section A, we have the effective sound speed, C_{eff}, in the presence of both types of plumes: β as well as γ. The term, C_{eff}, is expressed in terms of the real and imaginary components as:

$$C_{eff} = C_s + i\alpha_s \tag{19}$$

In Equation (19), the real component, C_s, represents the acoustic phase speed, and the imaginary component, α_s, represents the attenuation of the acoustic signal due to the presence of bubble plumes. Equation (12) is derived under the condition where multiple scattering among the bubbles is neglected. The two terms on the right side of Equation (19), can be, respectively, written as:

$$C_s = Re(C_{eff}) \tag{20}$$

$$\alpha_s(dB/m) = \frac{20}{In(10)} Im(\frac{1}{C_{eff}}) \tag{21}$$

From Fig. 5, we can infer that with the same increment in frequency, the acoustic signal is subjected to less resistance from the $\gamma-$plume induced region, compared to the region induced by both the $\beta-$ and $\gamma-$plumes. Alternatively, we can say that the acoustic signal propagates faster through the $\gamma-$plume induced region. From Fig. 6, we infer that the attenuation rate of acoustic signal is higher in the $\beta-$ and $\gamma-$plume induced region, than in the region with only $\gamma-$plume.

VI. Performance Evaluation

A. Simulation Settings

We have used NS-3 (http://www.nsnam.org/) for simulating our work. In our experiments, we have considered a shallow deployment region of dimension 200 $m \times$ 200 $m \times$ 200 m consisting of 10 nodes and 1 sink. Here, out the total 10 nodes, 5 nodes placed at the seabed act as source nodes. Other 5 nodes, which act as relay nodes, are placed uniformly over the simulation region. The sink node is placed at the sea-surface. We have adopted the *Ambient noise model* [27] for simulating the underwater channel and signal propagation. As explained in Section III, the source nodes periodically transmit packets to the sink node via the relay nodes. Other simulation parameters are shown in Table I.

TABLE I: Simulation Parameters

Parameters	**Values**
Bubble's Penetration Depth	$\beta-$plume: 1.4 - 2.1 m $\gamma-$plume: 7.1 - 8.3 m
Signal frequencies	10, 20, 30, 40 kHz
Simulation time	500 s
Packet interval	5 s
Modulation scheme	64-QAM
Wind speed (w_{10})	11–13 m/s
Transmit & receive power	0.203 & 0.024 $watts$ [28]

B. Performance Metrics

- *Packet Delivery Ratio* (*PDR*): PDR is expressed as the ratio of the *number of packets received* to the *number of packets send*. In our experiments, the source nodes placed at the sea-bed generate the packets and the sink node is the receiver of these packets.
- *Average Energy Consumption per Node*: Here, it is measured as the ratio of the total energy consumption of the network to the number of nodes. Mathematically,$\mathcal{E}_{avg} = \frac{1}{|N|}\sum_{i=1}^{|N|}\mathcal{E}_i$, where $|N|$ is the number of nodes and $\mathcal{E}_i$ is the energy consumption of node N_i.
- *Signal-to-Interference-Plus-Noise-Ratio* (*SINR*): SINR is the ratio of signal power to interference plus noise power. Mathematically, $SINR = \frac{\mathcal{S}_i}{\mathcal{I}+\mathcal{N}}$. Here, $\mathcal{S}_i$ is the signal power from the i^{th} source, $\mathcal{I}$ and $\mathcal{N}$ indicates the interference between the signals at the receiving end, and noise in the channel, respectively.
- *Bit Error Rate* (*BER*): In digital transmission, BER is defined as the ratio of percentage of bits with errors to the total no. of bits sent. In our experiments, we have used the 64-QAM modulation scheme for evaluating BER as in Ref. [29]: $BER = \frac{7}{12} \times (0.5 \times erfc(z))$.

C. Benchmark

We have compared the performance of our proposed scheme with the Thorp propagation [30] model for underwater environment. Thorp's model reflects the performance of UWASN where inter-node communication is affected due to attenuation of acoustic signal by conductive and saline ocean water. On the other hand, in our study, part of the channel, specifically the sub-surface region, is induced by bubble plumes. Hence, we have compared our simulation results with the results obtained using the Thorp model [30].

D. Results and Discussions

1) Packet Delivery Ratio (PDR): In Fig. 7, we have plotted the results for PDR in bubble free (Thorp's model) and bubble induced UWASNs. The results indicate that the PDR is 34% lower for bubble induced UWASNs, on an average. In bubble induced environment, signal absorption by bubble plumes effect in significant increase of the path loss. Hence, the packet delivery from source nodes to the sink hampers. However, in Thorp model, such signal impairment is not present, and thus, better PDR is observed. Also, for bubble induced UWASNs, PDR varies with the acoustic communication frequency. Except at 10 kHz, PDR increases with the increase in the communication frequency. This is due to the increase of signal path loss with increasing communication frequency for the bubble plume induced UWASNs.

2) Average Energy Consumption per Node: The average energy consumption per node for bubble free and bubble induced UWASNs are shown in Fig. 8. Comparing with the Thorp's model, the average energy consumption per node increases by 7% in bubble induced UWASNs. This is

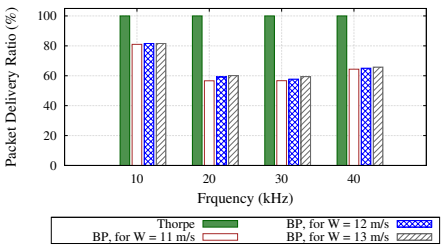

Fig. 7: Packet delivery ratio for bubble induced and bubble free channel

due to the fact that bubble induced UWASNs suffers from greater signal path loss. Moreover, with the increase in the acoustic communication frequency, the energy consumption also increases for bubble plume induced UWASNs. However, the change in average energy consumption is nearly similar for bubble free cases. With increase in the communication frequency, the signal path loss increases rapidly for bubble induced UWASNs that that for the bubble free cases. Hence, the average energy consumption per node increases with communication frequency.

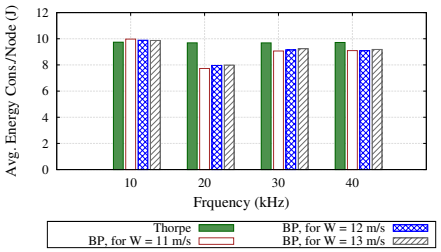

Fig. 8: Average energy consumption per node for bubble induced and bubble free channel

3) SINR: Fig. 9 shows the comparison of SINR results in bubble free and bubble induced regions. We see that for a specific communication frequency, SINR decreased by 53% for bubble induced UWASNs than that of the bubble free cases. However, with the change in acoustic communication frequency, the SINR values for bubble plume induced UWASNs remain nearly same. On the other hand, for bubble free UWASNs, the SINR values decrease with increase of communication frequency. This is because at higher frequencies, attenuation in Thorp's model increases which in turn decreases the SINR.

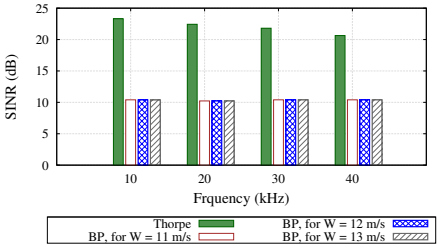

Fig. 9: SINR for bubble induced and bubble free channel

4) BER: We have plotted the results for BER varying the communication frequency in Fig. 10. A close observation reveals that, compared to Thorp, BER is higher in the bubble induced channel. Again, we see that BER gradually increases with the increase in the communciation frequency for bubble free UWASNs. Additionally, a comparative analysis reflects that as wind velocity shifts from 11-13 m/s, there is significant increase in the BER for bubble plume induced UWASNs. This is due to the fact that as the wind velocity increases, the bubble plumes penetrate more deeper region. Therefore, the signal travels more in the bubble plumes, where the propagation speed is lower. As expected, the bubble-induced channel invokes more errors in bits than the bubble-free channel. Overall, we infer that compared to Thorp, BER increases by 57%.

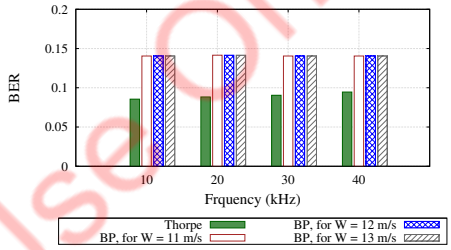

Fig. 10: BER for bubble induced and bubble free channel

VII. Conclusion

Under windy oceanic scenario, bubble plumes are important physical entities that persist near to the ocean surface. However, the existing works does not consider the effects of near-surface bubble plumes on the performance of UWASNs. In this work, we have studied the effects of near-surface bubble-induced region on network performance. The simulation results were evaluated comparing with the results obtained using the Thorp propagation model [30]. Compared to Thorp's model, the PDR was decreased by 34% while average energy consumption per node increases by 7%. Also, SINR decreases by approximately 53% and BER increases by 57%.

In future, we want to observe the effect of near-surface moving bubble plumes on the performance of distributed UWASNs, and also plan to perform field test experiments.

References

[1] I. F. Akyildiz, D. Pompili, T. Melodia, "Underwater acoustic sensor network: Research challenges," *Ad Hoc Netw.*, vol. 3, no. 3, pp. 257–279, 2005.

[2] J. Heidemann, M. Stojanovic, M. Zorzi, "Underwater sensor networks: applications, advances and challenges," *Phil. Trans. of The Royal Soc.*, vol. 370, pp. 158–175, 2012.

[3] S. Matsumae, "Energy-efficient cell partition of 3D space for sensor networks with location information," *Network Protocols and Algorithms*, vol. 1, no. 2, pp. 85–98, 2009.

[4] M. Garcia, S. Sendra, M. Atenas, and J. Lloret, *Mobile ad hoc networks: Current status and future trends*, 2011, ch. Underwater wireless ad-hoc networks: A survey, pp. 379–411.

[5] M. Garcia, S. Sendra, G. Lloret, and J. Lloret, "Monitoring and control sensor system for fish feeding in marine fish farms," *IET communications*, vol. 5, no. 12, pp. 1682–1690, 2011.

[6] M. Garcia, S. Sendra, J. Lloret, and A. Canovas, "Saving energy and improving communications using cooperative group-based wireless sensor networks," *Telecommunication Systems*, vol. 52, no. 4, pp. 2489–2502, 2013.

[7] S. Misra, T. Ojha, A. Mondal, "Game-theoretic topology control for opportunistic localization in sparse underwater sensor networks," *IEEE Trans. on Mobile Comp.*, vol. 14, no. 5, pp. 990–1003, 2015.

[8] D. Pompili, I. F. Akyildiz, "Overview of networking protocols for underwater wireless communications," *IEEE Comm. Mag.*, vol. 47, no. 1, pp. 97–102, 2009.

[9] A. K. Mandal, S. Misra, T. Ojha, M. K. Dash, M. S. Obaidat, "Oceanic forces and their impact on the performance of mobile underwater acoustic sensor networks," *Intl J. of Comm. Sys., Wiley*, 2014 [DOI: 10.1002/dac.2882].

[10] S. Pond, G. L. Pickard, *Introductory Dynamical Oceanography*, 2^{nd} ed. Butterworth-Heinemann, 1983.

[11] X. Lurton, *An introduction to underwater acoustics*, 1st ed., ser. Springer Praxis Books / Geophysical Sciences. Springer, December 2002.

[12] J. C. Novarini, R. S. Keiffer, G. V. Norton, "A model for variations in the range and depth dependence of the sound speed and attenuation induced by bubble clouds under wind-driven sea surfaces," *IEEE J. of Oceanic Engg.*, vol. 23, no. 4, pp. 423–438, October 1998.

[13] D. M. Farmer, G. B. Deane, S. Vagle, "The influence of bubble clouds on acoustic propagation in the surf zone," *IEEE J. of Oceanic Engg.*, vol. 26, no. 1, pp. 113–124, 2001.

[14] N. S. N. Ismail, L. A. Hussein, S. H. S. Ariffin, "Analyzing the performance of acoustic channel in underwater wireless sensor," in *Proc. of IEEE Intl. Conf. on Mathematical/Analytical Modelling and Comp. Simulation*, Kota Kinabalu, Malaysia, 2010, pp. 550–555.

[15] A. Stefanov, M. Stojanovic, "Design and performance analysis of underwater acoustic networks," *IEEE J. of Oceanic Engineering*, vol. 29, no. 10, pp. 2012–2021, 2011.

[16] A. K. Mandal, S. Misra, M. K. Dash, "Effect of near-surface bubble plumes on the acoustic signal used in UWACNs," in *Proc. of Intl. Conf. on Wireless Comm. and Mob. Comp.*, Italy, 2013, pp. 1816–1820.

[17] W. L. J. Fox, P. Arabshahi, S. Roy, N. Parrish, "Underwater acoustic communications performance modeling in support of ad hoc network design," in *Proc. of MTS/IEEE Oceans*, Vancouver, BC, 2007, pp. 1–5.

[18] J. Llor, M. P. Malumbres, "Underwater wireless sensor networks: How do acoustic propagation models impact the performance of higher-level protocols?" *J. of Sensors*, vol. 12, no. 2, pp. 1312–1335, 2012.

[19] W. Zhang, M. Stojanovic, U. Mitra, "Analysis of a linear mulihop underwate acoustic network," *IEEE J. of Oceanic Engg.*, pp. 1–10, 2010.

[20] S. A. Thorpe, "On the clouds of bubbles formed by breaking waves in deep water and their role in the air-sea gas transfer," *Philos. Trans. R. Soc. London Ser. A*, vol. 304, pp. 155–210, 1982.

[21] E. C. Monahan, *Natural Physical Sources of Underwater Sound*, B. R. Kerman, Ed. Boston, MA: Kluwer, 1993.

[22] M. V. Hall, "A comprehensive model of wind-generated bubbles in the ocean and predictions of the effects on sound propagation at frequencies up to 40 kHz," *J. of Acoust. Soc. of Am.*, vol. 86, pp. 1103–1116, 1989.

[23] U. Saxena, P. K. Bhaskaran, "A bubble population density spectrum for central arabian sea," *J. of Ship Technology*, vol. 6, no. 2, 2010.

[24] E. C. Monahan, O. Muircheartaigh, "Optimal power-law description of oceanic whitecap coverage dependence on wind speed," *J. of Phys. Ocean.*, vol. 10, pp. 2094–2099, 1980.

[25] E. L. Andreas, E. C. Monahan, "The role of whitecap bubbles in air-sea heat and moisture exchange," *J. of Phy. Ocean.*, vol. 30, pp. 433–442, 2000.

[26] E. C. Monahan, M. Lu, "Acoustically relevant bubble assemblages and their dependence on meteorological parameters," *IEEE J. of Oceanic Engg.*, vol. 15, no. 4, pp. 340–349, 1990.

[27] A. F. Harris, M. Zorzi, "Modeling the underwater acoustic channel in ns2," in *Proc. of the 2^{nd} Intl. Conf. on Performance Evaluation Methodologies and Tools*, Nantes, France, 2007.

[28] A. Sanchez, S. Blanc, P. Yuste, J. J. Serrano, "A low cost and high efficient acoustic modem for underwater sensor networks," in *Proc. of MTS/IEEE OCEANS*, 2011, pp. 1–10.

[29] B. A. Forouzan, *Data Communication and Networking*, 4th ed. McGraw-Hill, February 2006.

[30] W. H. Thorp, "Analytic description of the low frequency attenuation coefficient," *J. of Acoustical Soc. of America*, p. 270, 1967.